Check for updates

EurJOC
European Journal of Organic Chemistry

Research Article
doi.org/10.1002/ejoc.202500669

Chemistry Europe
European Chemical Societies Publishing

www.eurjoc.org

[3]Radialene Fluorophores with pH-Switchable Emission and Stable Absorption Maxima

Jan P. Soyka, J. Felix Witte, Anja Wiesner, Alexander R. Krappe, Dana Wehner, Nicola Alnicola, Beate Paulus, Ute Resch-Genger, and Siegfried Eigler*

The first push–pull quino [3]radialene fluorescent dye is reported. Herein, the novel bis(dicyanomethylene)-[3]radialene electron acceptor is connected to a benzimidazole donor. With protonation, a substantial redshift of fluorescence wavelength is observed, while the absorption maximum remains stable. This process is accompanied with an increased fluorescence quantum yield to about 70%. Further, the findings are explained by a combined experimental and theoretical approach, and it is found that vibronic coupling plays a crucial role. This study highlights the yet unexplored potential of [3]radialene-based motifs for the design of environment-responsive fluorophores.

1. Introduction

Fluorophores have diverse applications, e.g., in optoelectronic devices,[1] such as organic light emitting diodes in TV screens,[2–4] in bioimaging,[5] or as sensors.[6–8] Introducing functional groups in proximity to chromophore units can dramatically alter excited-state dynamics. Many small molecular dyes contain benzene-based push–pull motifs and were presented in the last decade.[9–11] In contrast, the benzene isomer [3]radialene (**1**, **Figure 1**) had not been extensively investigated yet. [3]radialenes are a class of alicyclic hydrocarbons consisting of sp^2–hybridized carbon atoms, each bearing an exocyclic double bond on each carbon atom.[12] These cross-conjugated exocyclic double bonds exhibit weak aromaticity within their cyclic substructures[13,14] and can act as chromophores.[6,15,16] For the design of dyes, often push–pull systems are integrated into the molecular structure. In this context, the electron–poor tris(dicyanomethylene)-[3]radialene (CN6–CP, **2**) possesses an exceptionally high electron affinity of $E = 5.94$ eV versus Ag/Ag^+.[17]

We recently exploited this property to generate high vertical electric fields in 2D heterostructures.[17] Moreover, CN6-CP is currently examined to serve as an efficient organic electron acceptor.[18–21] We thus expect the CN6-CP to act as a suitable electron-accepting moiety in push–pull systems. Additionally, we recently reported on a novel class of fluorescent dyes containing a dimethylene-cyclopropanide moiety,[22–24] which we utilized in various fluorescent dyes, e.g., the DMAP derivative **3**.[25]

Furthermore, we described a potential class of compounds for nonlinear optics, incorporating diaminodicyano-quinodimethane (DADQ) as a fluorophore motif, in which an imidazole unit acts as a donor.[26–28] This class of dyes exhibits unusual photophysical properties such as the formation of metastable dimers as a result of their high dipole moments. DADQ compounds feature a quinone system embedded in a donor–acceptor periphery (**4**, Figure 1). This unique structure provides fluorescence quantum yields (Φ_{fl}) of up to 90% in DMSO.[27,29,30] Herein, we combine the previously introduced motifs by replacing the electron-withdrawing malononitrile group of the DADQ derivative **4** with the bis(dicyanomethylene)-[3]radialene moiety of **2** respectively **3**, resulting in the novel push–pull quino [3]radialene compound **5a**. To the best of our knowledge, compound **5a** is the first reported push–pull [3]radialene.[15,16,31] We validate the molecular structure using single-crystal X-ray diffraction and investigate the photophysical properties of this compound upon protonation. The protonation-induced changes in fluorescence quantum yield and redshift of the wavelength highlight the potential of this class as fluorescent probes and sensors.

2. Results and Discussion

To combine the [3]radialene motif with the DADQ system, we followed a convergent synthesis strategy depicted in **Figure 2**A.

J. P. Soyka, A. R. Krappe, D. Wehner, S. Eigler
Institut für Chemie und Biochemie (SupraFAB)
Freie Universität Berlin
Altensteinstraße 23a, 14195 Berlin, Germany
E-mail: siegfried.eigler@fu-berlin.de

J. F. Witte, N. Alnicola, B. Paulus
Institut für Chemie und Biochemie
Freie Universität Berlin
Arnimallee 22, 14195 Berlin, Germany

A. Wiesner
Institut für Chemie und Biochemie
Freie Universität Berlin
Fabeckstraße 34/36, 14195 Berlin, Germany

U. Resch-Genger
Bundesanstalt für Materialforschung und -prüfung (BAM), Department 1
Division Biophotonics
Richard-Willstätter-Straße 11, 12489 Berlin, Germany

Supporting information for this article is available on the WWW under https://doi.org/10.1002/ejoc.202500669

© 2025 The Author(s). European Journal of Organic Chemistry published by Wiley-VCH GmbH. This is an open access article under the terms of the Creative Commons Attribution License, which permits use, distribution and reproduction in any medium, provided the original work is properly cited.

© 2025 The Author(s). European Journal of Organic Chemistry published by Wiley-VCH GmbH

Research Article
doi.org/10.1002/ejoc.202500669

Chemistry Europe
European Chemical Societies Publishing

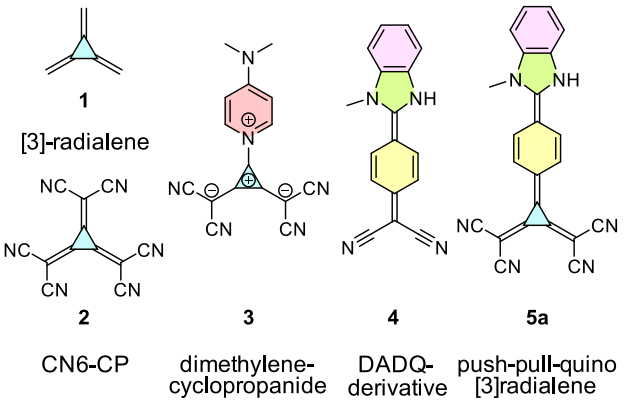

Figure 1. Structural motif of a [3]radialene (**1**), the strong electron acceptor tris(dicyanomethylene)-[3]radialene (CN6-CP, **2**), a dimethylene-cyclopropanide containing fluorescent dye **3**, a methyl-substituted diamino-dicyano-quinodimethane (Me-DADQ) derivative **4**, and the combined product compound, a push–pull quino [3]radialene **5**.

First, the 4-iodophenyl-*N*-methyl-benzimidazole **7** was synthesized by condensation of 4–iodobenzoic acid **6** and 1,2–diaminobenzene, followed by methylation. In the course of the synthesis, we realized that methylation of compound **7** is essential for increasing the yield of subsequent reactions. As coupling partner of the methylated compound **8**, the triethylamine-substituted cyclopropene **10** was synthesized from tetrachlorocyclopropene (TCCP).[22] TCCP itself was synthesized according to the literature.[32] After metal–halogen exchange in **8** employing *n*-butyl lithium, nucleophilic substitution with **10** yields compound **5a** with >99.5% purity (Figure 2).

The chemical structure could be confirmed by single-crystal X-ray diffraction, mass spectrometry, and NMR spectroscopy. As depicted in **Figure 3**, substituents can be introduced at the imidazole moiety. Accordingly, the series of compounds **5a**–**5e** was synthesized (see Supporting Information for detailed information). We note that cleavage of the amine-protecting groups under standard conditions, e.g., acidic conditions for **5d** and **5e** or hydrogenation for **5b** and **5d**, leads to complex product mixtures. A similar behavior was also observed for related DADQ derivatives (Table S1–S3, Supporting Information).

The solid-state structure of **5a**[33] is shown in Figure 2B and Figure S24, Supporting Information. It crystallizes in space group $P2_1/n$ with four molecules per unit cell. The intermolecular distance is ≈3.6 Å. The central benzene ring C (Figure 2B) displays a very weak *para*-quinoid geometry (Figure S24, Supporting Information). Notably, the bonds to rings B (1.462(2) Å) and D (1.442(2) Å) are elongated, and the molecule exhibits significant torsion around α (Figure 2B), with a dihedral angle of 36.8°. These features are similar to those in DADQ **4b** (Figure S25, Supporting Information). The [3]radialene ring is distorted, with shorter bonds adjacent to the quinone (1.376/1.374 Å) compared to the bond between malononitrile units (1.413 Å), consistent with

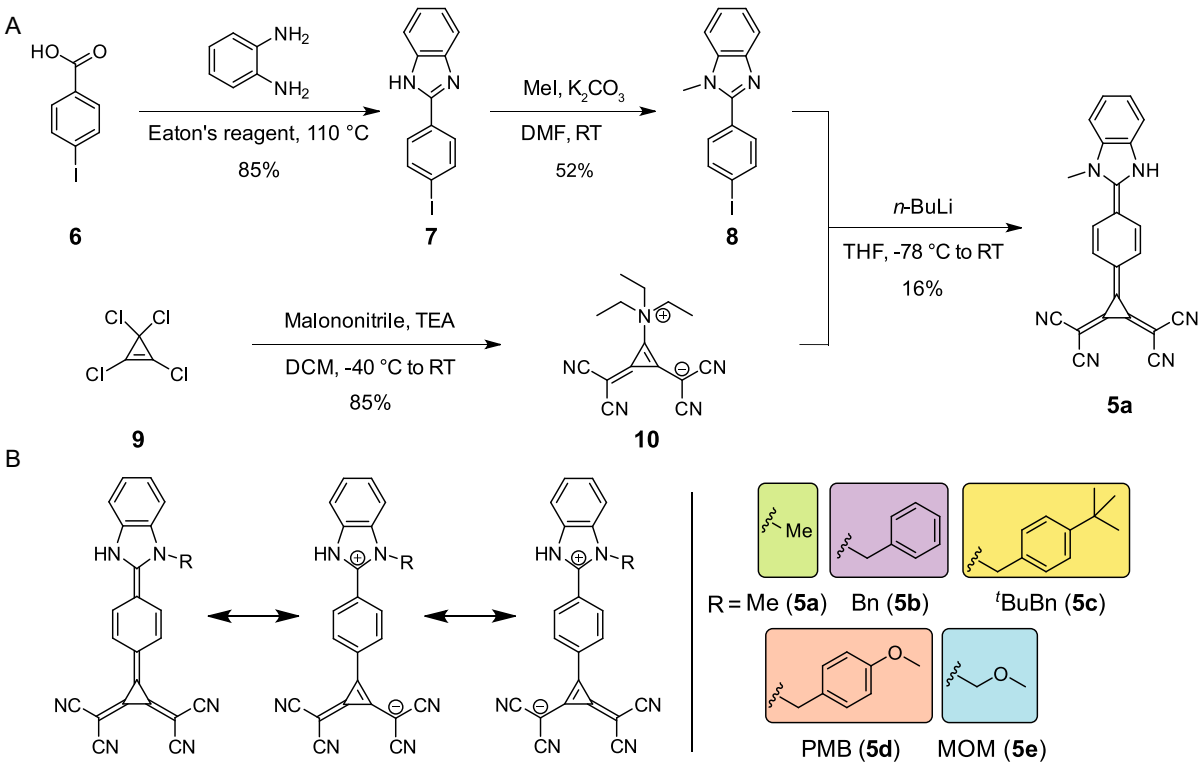

Figure 2. A) Synthesis of push–pull [3]radialene **5a** starting from 4-iodobenzoic acid, which was condensed with 1,2-diaminobenzene to the corresponding benzimidazole and methylated subsequently. The 2,3–bis(dicyanomethylene)-cyclopropan-1-ylium (CN4-CP)-electron-withdrawing group was obtained from tetrachlorocyclopropene (TCCP) by substitution with malononitrile. Coupling was achieved by a lithium-iodide exchange of **8** with *n*-BuLi and subsequent attack of compound **10** to yield **5a**. B) Overview of different exemplary mesmeric structures and residues for the push–pull quino [3]radialene. Calculations of electronic properties as well as synthetic protocols and photophysical properties are reported in the Supporting Information.

© 2025 The Author(s). European Journal of Organic Chemistry published by Wiley-VCH GmbH

Research Article
doi.org/10.1002/ejoc.202500669

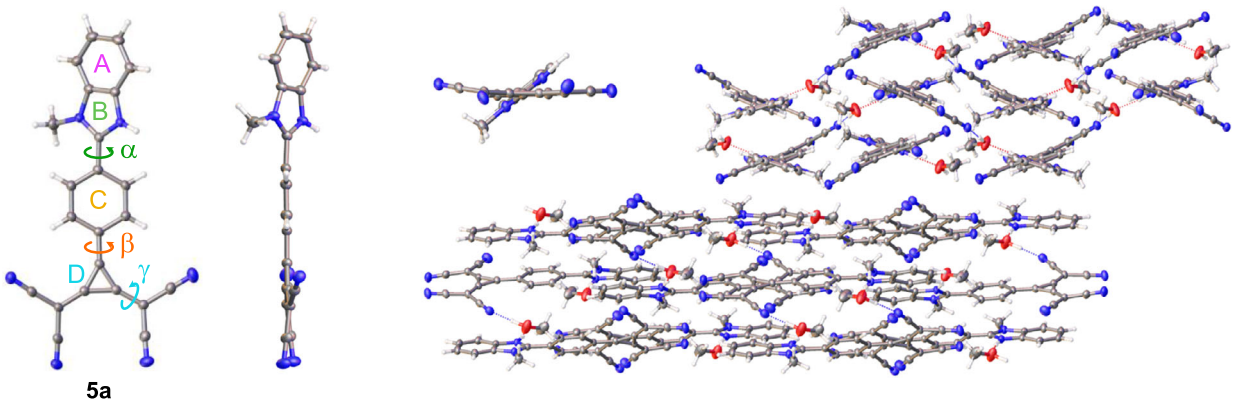

Figure 3. Molecular structure in the solid state of **5a** viewed from all axes and the 3D packing with cocrystallized MeOH.[33] Thermal ellipsoids are shown at 50% probability level. Carbon is gray, nitrogen is blue, and hydrogen is white.

previous reports.[25] The resolved bond lengths indicate neither a clear quinoid nor an aromatic character. Thus, for a better understanding of the aromaticity in **5a**, we calculated the nucleus independent chemical shift NICS(1)$_{zz}$[34,35] values, which indicate an aromatic character for all rings labeled in Figure 2B in the ground state, although less aromatic compared to benzene (Table S17, Supporting Information). Remarkably, only ring A shows a strong diatropic ring current, while rings B, C, and D exhibit weaker currents, with NICS values lower than those of the respective isolated rings.[6,13,36,37] Further discussion of the NICS values, the σ−aromaticity of ring D, and the highest occupied and lowest unoccupied molecular orbitals (HOMOs and LUMOs) is provided in Figure 7 and **Table 1** as well as in the SI (Figure S21,S23, Table S18, Supporting Information).[27,38]

Table 1. Calculated NICS(0), NICS (1), and NICS(1)$_{zz}$ of 5a. Values were calculated on the B3LYP/def2-TZVP level of theory. The geometry was optimized at the ωB97XD/def2-TZVP level of theory.

Ring	NICS(0)	NICS(1)	NICS(1)$_{zz}$
A	−10.06	−10.69	−22.93
B	−9.36	−6.53	−12.78
C	−4.00	−6.21	−14.67
D	−25.75	−8.79	−13.16

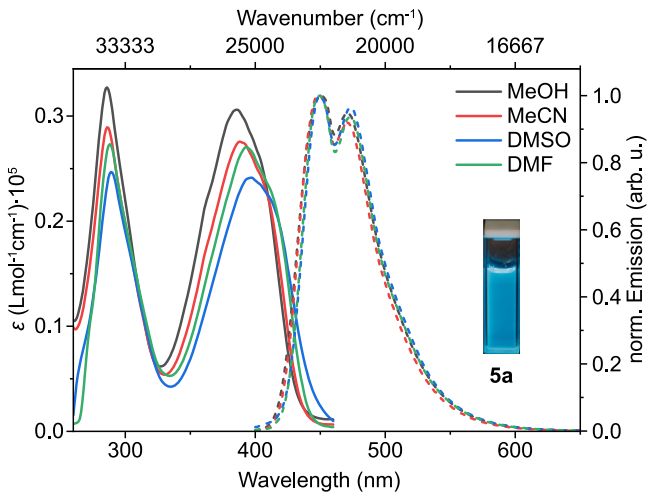

Figure 4. Absorption (solid line) and emission (dashed line) spectra of **5a** in MeOH (black), MeCN (red), DMSO (blue), DMF (green). Excitation was performed at the respective second absorption maximum for each solvent.

The absorption spectra of **5a** (**Figure 4**, Figure S4, Supporting Information) exhibit two maxima at about 285 nm and 390 nm with molar absorption coefficients between 24 000 and 35 000 L mol^{-1} cm^{-1} depending on the solvent. According to time-dependent density functional theory calculations (Table S15, Supporting Information), the absorption peak at 390 nm corresponds to the S_0–S_1 transition and involves the transition from the HOMO to the LUMO. The absorption band at higher energies results primarily from a transition from the HOMO −1 to LUMO. The absorption maximum displays only a small dependence on solvent polarity and proticity, indicating that the molecular dipole moment changes only little upon excitation. A similar effect was found for Me-DADQ (**4**).[30] However, although we discovered the formation of metastable dimers for compound **4**, the compound **5a** does not show this behavior (see concentration-dependent absorption studies in SI, Figure S4E, S10, Supporting Information).[27,29,30]

The emission spectra of the push–pull quino[3]radialene **5a** display a vibronic fine structure with two maxima at 449 nm and 472 nm (Figure 4), which we attribute to vibronic coupling. We note that the different substituents of compounds **5a**–**5e** have no noteworthy impact on the photophysical properties (Figure S7–10, Supporting Information).

We determined short lifetimes of about 0.2 ns; however, the fluorescence quantum yields (Φ_{fl}) of **5a** are relatively low and vary between 7% and 22% in solutions and 2% in solids. This behavior indicates rapidly competing nonradiative decay pathways, which we attribute to rotations and identified by viscosity-dependent measurements (see detailed discussion in Table S7, S8, Figure S6, Supporting Information).

Most striking are the changes of fluorescence properties observed upon protonation of compound **5a**. By adding HCl$_{aq}$ to a DMSO solution of the dye, the spectral shape and intensity

© 2025 The Author(s). European Journal of Organic Chemistry published by Wiley-VCH GmbH

Research Article
doi.org/10.1002/ejoc.202500669

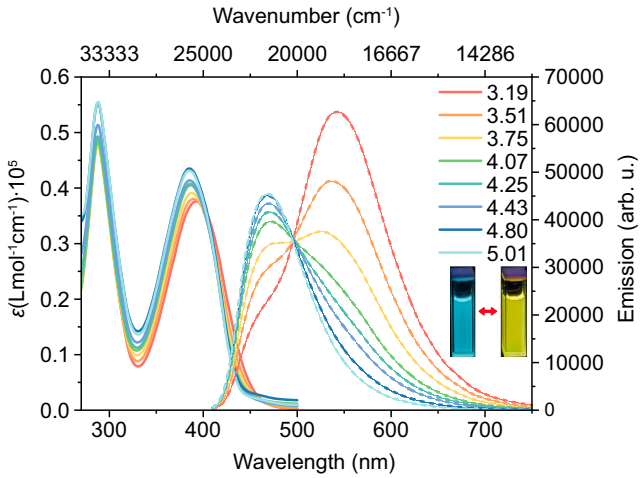

Figure 5. Titration of **5a** using a DMSO/BR buffer solution with different pH values shows an increased fluorescence quantum yield Φ_{fl} and a shift of the emission wavelength to longer wavelengths.

of absorption spectra are barely affected. However, protonation leads to the appearance of a new redshifted emission band at 543 nm, accompanied by a strong increase in Φ_{fl} (**Figure 5**) from 22% in DMSO to 71% in DMSO/1% of 37% HCl_{aq} (Table S9, Supporting Information). This reflects a 3.2-fold enhancement. Titration experiments of the compound with a Britton–Robinson (BR) buffer reveal a pK_a value of 3.8 for **5aH**$^+$. The observation of an isosbestic point at 495 nm indicates the presence of two species and a straightforward protonation reaction without side products. According to the charge population analysis for compound **5a** using the minimal basis iterative stockholder method, a variation of the Hirshfeld method,[39] the methylene carbon of the malononitrile group carries the largest amount of negative charge, making it the most likely site for protonation (Figure S18 and Table S16, Supporting Information).

Since fluorescent push–pull [3]radialenes are a novel class of fluorescent dyes, we performed quantum chemical calculations to explain the photophysical properties. Structural freedom or rigidity is often a key factor in rationalizing spectroscopic properties, particularly fluorescence features.[27,29,30] As mentioned before, we assessed rotations in compound **5a** by conducting (relaxed) potential energy surface scans for the ground state and the first excited state at dihedral angles α, β, and γ (Figure S15 and 2B, Supporting Information, left). The scan at γ indicates a very shallow second minimum at 90°, but the corresponding transition energy (675 nm) clearly deviates from the experimental data, and the oscillator strength of the S_0–S_1 transition approaches zero. Nevertheless, these calculations support that the observed fluorescence bands at about 450 nm and 470 nm originate from the coupling of electronic states and vibrational motions. Therefore, we used the excited-state dynamic module of ORCA package and calculated the ground- and excited-state Hessians of the respective optimized structures. Subsequently, an excited-state dynamics run was performed using a path integral approach suggested by de Souza et al.[40] The resulting fluorescence spectrum shown in **Figure 6** agrees relatively well with

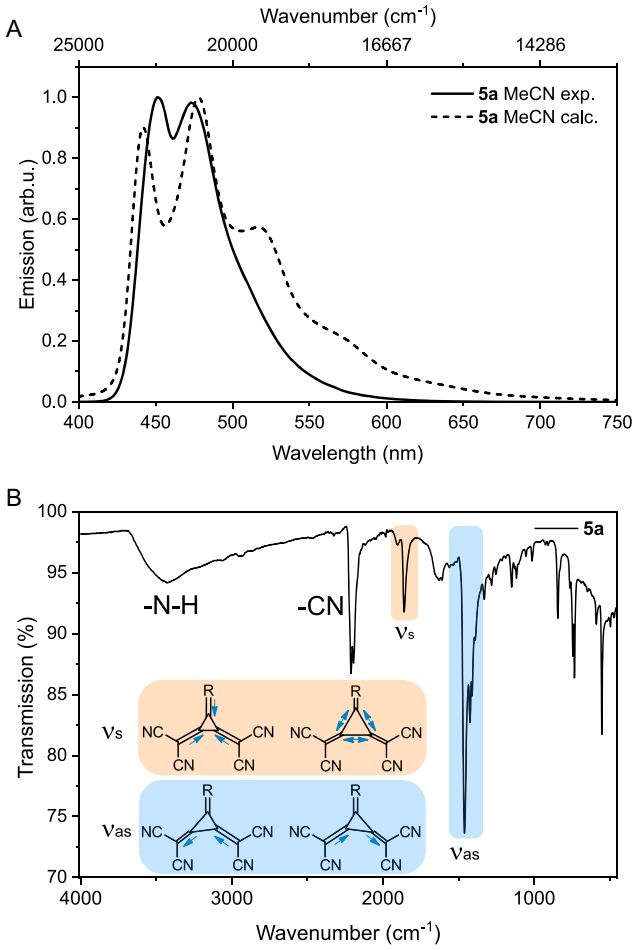

Figure 6. A) Calculated emission spectra (dashed line) and measured emission spectra (solid line) of **5a**. B) IR spectrum of **5a** featuring two distinct vibrational bands from the cyclopropane ring, the symmetric (orange) and asymmetric (blue) valence vibrations.

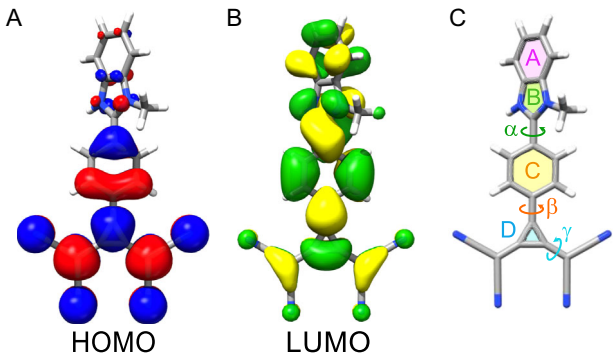

Figure 7. A) HOMO and B) LUMO of **5a** calculated at the ωB97X-D3/def2-TZVP level in MeCN, isovalue = ±0.015 $a_0^{-3/2}$ C) shows **5a** with the rings A to D and the three possible rotation axes.

the experimental one in MeCN. Further, we identify the three-membered ring playing a crucial role in the shape of bands. The Fourier transform infrared (FTIR) spectrum of compound **5a** shows distinct peaks of the [3]radialene and the nitrile groups, while other vibrational modes appear with negligible intensity

© 2025 The Author(s). European Journal of Organic Chemistry published by Wiley-VCH GmbH

(Figure 6B). The calculated apparent band splitting of ≈1800 cm^{-1} can be attributed to the coupling of the electronic S_1–S_0 transition to the vibrational modes of the three-membered ring. The experimental band splitting is 1200 cm^{-1} and thus supports that the vibrational progression originates from the coupling with the symmetric mode, measured at 1860 cm^{-1}, and the asymmetric mode at 1462 cm^{-1} of the three-membered ring (Figure S16, Supporting Information). The results highlight the unique properties of the [3]radialene motif, which is dominant compared to the related DADQ structures.[6,27]

However, in the case of protonated **5aH**$^+$ (see Figure 5), the bands of the calculated IR spectrum of the S_0 state also contain contributions from the quinoid system. More importantly, in the S_1 state manifold, intense combination bands dominate the spectrum (Figure S20, Supporting Information). As a result, the vibrational coupling leads to the broad and continuous emission between 500 and 700 nm (Figure 5). Comparing the optimized geometries of the neutral **5a** and protonated **5aH**$^+$ in both the S_0 and S_1 states suggest that the reduced torsion angle α leads to better π-orbital overlap and enhanced delocalization in the first excited state. This partially explains the observed redshift in the emission upon protonation. The absence of a shift in the absorption spectra of **5a** and **5aH**$^+$ can be explained by the torsion α not affecting the π-overlap in the S_0 state (Figure S20, Supporting Information).

To gain a deeper understanding of the electronic structure, we calculated the frontier molecular orbitals (HOMO and LUMO) at the ωB97X-D3/def2-TZVP level of theory using the conductor-like polarizable continuum model, simulating the dielectric constant corresponding to acetonitrile (see **Figure 7**). Unusual for classical push–pull fluorophores, the HOMO is predominantly localized on the electron-accepting moiety. In contrast, the LUMO shows more electron density on the donor-substituted imidazole unit, while being primarily delocalized over the entire π-system. We attribute this reversed orbital character to the significant ground-state dipole moment with a calculated dipole moment of 45.9 D at the ωB97X-D3/aug-cc-pVTZ level of theory, which remains high upon excitation (S_1: 44.4 D). The HOMO energy of ≈–5.6 eV alone does not explain the unusual localization of electron density on the acceptor, indicating that a pre-existing ground-state charge separation is the more plausible explanation. This interpretation is consistent with the absence of pronounced solvatochromism and suggests that no classical intramolecular charge transfer occurs upon excitation, as the charge-separated state is already established in S_0.

Radialenes[13] possess low aromaticity, whereas triafulvene[36] exhibits an aromatic character. The NICS(1)$_{zz}$[34,35] values for compound **5a** indicate an aromatic character for all ring substructures (Figure 7C) in the ground state (see Table 1). Remarkably, only ring system A shows a strong diatropic ring current, whereas ring systems B, C, and D exhibit only weak ring currents, which are considerably lower than for imidazole, benzene, and [3]radialene only.[6,37] Compared with DADQ **4** (Table S18, Supporting Information), the aromaticity in the rings B and C in **5a** is slightly stronger than in the corresponding rings of **4**.[27] To assess the σ−aromaticity and improve the understanding of the system's aromaticity, we focused solely on the σ−electron framework by excluding π–contributions (Figure S23, Supporting Information).[38] Herein, we observed a comparably large σ–contribution in the anisotropies of ring D, typical for cyclopropanes.

3. Conclusion

We have investigated the influence of the electron-withdrawing group 2,3–bis(dicyanomethylene)-cyclopropan-1-ylium (CN4-CP), a radialene-like electron-withdrawing motif, on the photophysical properties of compound **5a**. A new synthetic approach was developed to construct [3]radialenes covalently connected via a C—C bond to a quinone unit, and we obtained the first push–pull radialene fluorescent dye, reported so far, which presents a push–pull system with a CN4–CP electron acceptor and a benzimidazole donor. Single-crystal X-ray diffraction was used to prove the connectivity, bond lengths, and dihedral angles.

Spectroscopic studies of the influence of the electron-withdrawing group 2,3–bis(dicyanomethylene)-cyclopropan-1-ylium (CN4-CP), a radialene-like electron-withdrawing motif, on the photophysical properties of compound **5a** in solvents of different polarity, proticity, and viscosity revealed only a small sensitivity of the absorption properties to dye microenvironment. This was attributed to the similarly high dipole moments of the dye in the S_0 (45.9 D) and S_1 (44.4 D) states. The emission, which is also barely affected by polarity, shows a pronounced vibrational progression, which is dominated by the strong vibrational modes of the [3]radialene motif. An increase in solvent viscosity by addition of PEG 400 led to an increase in fluorescence quantum yield Φ_{fl} by a factor of about 2, suggesting rotation caused nonradiative pathways. Most striking, the dye's fluorescence quantum yield increased to 71% upon protonation, accompanied by the appearance of a new redshifted emission band at 543 nm, while the absorption spectrum remained almost unaffected. We attribute the shift of emission wavelength to improved π-conjugation as a consequence of lower torsion of the system. In addition, we show that the broad emission band is due to the more intense vibrational combination modes. These modes are activated by protonation. Our findings underscore the potential of [3]radialene-based motifs in fluorophores and open avenues for new sensing applications, such as pH values.

Acknowledgements

The authors gratefully acknowledge funding by the Deutsche Forschungsgemeinschaft (DFG, German Research Foundation) for projects 530311849 (S.E., J.P.S., and U.R.G.) and RE 1203/45–1 and RE 1203/46–1 (U.R.G.). The authors would like to thank the HPC Service of FUB-IT, Freie Universität Berlin, for computing time (10.17169/refubium-26754). The authors thank Arne Güttler (BAM) for insightful discussions and assistance with measurements.

Open Access funding enabled and organized by Projekt DEAL.

© 2025 The Author(s). European Journal of Organic Chemistry published by Wiley-VCH GmbH

Conflict of Interest

The authors declare no conflict of interest.

Data Availability Statement

The data that support the findings of this study are openly available in Refubium (Freie Universität Berlin) at https://doi.org/10.17169/refubium-47131/.

Keywords: [3]radialene · dipole · dyes · fluorescence · sensors

[1] G. Hong, X. Gan, C. Leonhardt, Z. Zhang, J. Seibert, J. M. Busch, S. Bräse, *Adv. Mater.* **2021**, *33*, 2005630.
[2] Y. Li, J.-Y. Liu, Y.-D. Zhao, Y.-C. Cao, *Mater. Today* **2017**, *20*, 258.
[3] Y. Liu, B. Nell, K. Ortstein, Z. Wu, Y. Karpov, T. Beryozkina, S. Lenk, A. Kiriy, K. Leo, S. Reineke, *ACS Appl. Mater. Interfaces* **2019**, *11*, 11660.
[4] A. L. Antaris, H. Chen, S. Diao, Z. Ma, Z. Zhang, S. Zhu, J. Wang, A. X. Lozano, Q. Fan, L. Chew, M. Zhu, K. Cheng, X. Hong, H. Dai, Z. Cheng, *Nat. Commun.* **2017**, *8*, 15269.
[5] Q. Shen, S. Wang, N.-D. Yang, C. Zhang, Q. Wu, C. Yu, *J. Lumin.* **2020**, *225*, 117338.
[6] G. Xu, H. Liu, Z. Zhou, W. Lai, B. Li, Y. Zhou, R. Hu, W. Yao, K. Yang, S. Xie, Z. Zeng, *Angew. Chem. Int. Ed.* **2023**, *62*, e202305011.
[7] P. Srivastava, I. Tavernaro, L. Scholtz, C. Genger, P. Welker, F. Schreiber, K. Meyer, U. Resch-Genger, *Sci. Rep.* **2023**, *13*, 1321.
[8] T. Reiber, O. Hübner, C. Dose, D. A. Yushchenko, U. Resch-Genger, *Sci. Rep.* **2024**, *14*, 11882.
[9] H. Liu, S. Yan, R. Huang, Z. Gao, G. Wang, L. Ding, Y. Fang, *Chem.-Eur. J.* **2019**, *25*, 16732.
[10] E. Yamaguchi, C. Wang, A. Fukazawa, M. Taki, Y. Sato, T. Sasaki, M. Ueda, N. Sasaki, T. Higashiyama, S. Yamaguchi, *Angew. Chem. Int. Ed.* **2015**, *54*, 4539.
[11] J. Wudarczyk, G. Papamokos, V. Margaritis, D. Schollmeyer, F. Hinkel, M. Baumgarten, G. Floudas, K. Müllen, *Angew. Chem. Int. Ed.* **2016**, *55*, 3220.
[12] H. Hopf, G. Maas, *Angew. Chem. Int. Ed.* **1992**, *31*, 931.
[13] J. R. Dias, *Mol. Phys.* **2017**, *115*, 771.
[14] C. Lepetit, M. Brøndsted Nielsen, F. Diederich, R. Chauvin, *Chem.-Eur. J.* **2003**, *9*, 5056.
[15] J. Yu, C. Tang, X. Gu, X. Zheng, Z.-Q. Yu, Z. He, X.-G. Li, B. Z. Tang, *Chem. Commun.* **2020**, *56*, 3911.
[16] A. Avellaneda, C. A. Hollis, X. He, C. J. Sumby, *Beilstein J. Org. Chem.* **2012**, *8*, 71.
[17] K. Bolotin, S. Kovalchuk, K. Greben, A. Kumar, S. Pessel, J. Soyka, Q. Cao, K. Watanabe, T. Taniguchi, D. Christiansen, M. Selig, A. Knorr, S. Eigler, *New interlayer excitons in 2D bilayers revealed under strong electric field*, Research Square preprint **2023**, https://doi.org/10.21203/rs.21203.rs-3453831/v3453831.
[18] Y. Karpov, N. Kiriy, P. Formanek, C. Hoffmann, T. Beryozkina, M. Hambsch, M. Al-Hussein, S. C. B. Mannsfeld, B. Büchner, B. Debnath, M. Bretschneider, Y. Krupskaya, F. Lissel, A. Kiriy, *Adv. Electron. Mater.* **2020**, *6*, 1901346.
[19] Y. Karpov, T. Erdmann, I. Raguzin, M. Al-Hussein, M. Binner, U. Lappan, M. Stamm, K. L. Gerasimov, T. Beryozkina, V. Bakulev, D. V. Anokhin, D. A. Ivanov, F. Günther, S. Gemming, G. Seifert, B. Voit, R. Di Pietro, A. Kiriy, *Adv. Mater.* **2016**, *28*, 6003.
[20] J. Saska, N. E. Shevchenko, G. Gonel, Z. I. Bedolla-Valdez, R. M. Talbot, A. J. Moulé, M. Mascal, *J. Mater. Chem. C* **2021**, *9*, 15990.
[21] H. L. Smith, J. T. Dull, S. K. Mohapatra, K. Al Kurdi, S. Barlow, S. R. Marder, B. P. Rand, A. Kahn, *ACS Appl. Mater. Interfaces* **2022**, *14*, 2381.
[22] J. M. Holthoff, E. Engelage, R. Weiss, S. M. Huber, *Angew. Chem. Int. Ed.* **2020**, *59*, 11150.
[23] J. M. Holthoff, R. Weiss, S. V. Rosokha, S. M. Huber, *Chem.–Eur. J.* **2021**, *27*, 16530.
[24] C. Loy, J. M. Holthoff, R. Weiss, S. M. Huber, S. V. Rosokha, *Chem. Sci.* **2021**, *12*, 8246.
[25] M. Yanbaeva, J. Soyka, J. M. Holthoff, P. Rietsch, E. Engelage, A. Ruff, U. Resch-Genger, R. Weiss, S. Eigler, S. M. Huber, *Chem.–Eur. J.* **2024**, *30*, e202402476.
[26] S. Jayanty, T. P. Radhakrishnan, *Chem.–Eur. J.* **2004**, *10*, 791.
[27] P. Rietsch, F. Witte, S. Sobottka, G. Germer, A. Krappe, A. Güttler, B. Sarkar, B. Paulus, U. Resch-Genger, S. Eigler, *Angew. Chem. Int. Ed.* **2019**, *58*, 8235.
[28] C. G. Chandaluri, T. P. Radhakrishnan, *Opt. Mater.* **2011**, *34*, 119.
[29] F. Witte, P. Rietsch, N. Nirmalananthan-Budau, F. Weigert, J. P. Götze, U. Resch-Genger, S. Eigler, B. Paulus, *Phys. Chem. Chem. Phys.* **2021**, *23*, 17521.
[30] F. Witte, P. Rietsch, S. Sinha, A. Krappe, J.-O. Joswig, J. P. Götze, N. Nirmalananthan-Budau, U. Resch-Genger, S. Eigler, B. Paulus, *J. Phys. Chem. B* **2021**, *125*, 4438.
[31] P. K. Sharma, D. Mallick, S. Das, *Org. Lett.* **2023**, *25*, 5089.
[32] J. Sepiol, R. L. Soulen, *J. Org. Chem.* **1975**, *40*, 3791.
[33] Deposition numbers 2440484 (for **5a**) and 2440486 (for **4c**) contain the supplementary crystallographic data for this paper, *these Data are Provided Free of Charge by the Joint Cambridge Crystallographic Data Centre ad Fachinformationszentrum Karlsruhe Access Structures Service.*
[34] A. Stanger, *Eur. J. Org. Chem.* **2020**, *2020*, 3120.
[35] A. Stanger, *J. Org. Chem.* **2006**, *71*, 883.
[36] A. Tokatlı, F. Tunç, F. Ucun, H. Oturak, *Phosphorus, Sulfur Silicon Relat. Elem.* **2017**, *192*, 351.
[37] J. Elguero, I. Alkorta, R. M. Claramunt, P. Cabildo, P. Cornago, M. Á. Farrán, M. Á. García, C. López, M. Pérez-Torralba, D. S. María, D. Sanz, *Chem. Heterocycl. Compd.* **2013**, *49*, 177.
[38] A. Stanger, *J. Org. Chem.* **2010**, *75*, 2281.
[39] T. Verstraelen, S. Vandenbrande, F. Heidar-Zadeh, L. Vanduyfhuys, V. Van Speybroeck, M. Waroquier, P. W. Ayers, *J. Chem. Theory Comput.* **2016**, *12*, 3894.
[40] B. de Souza, F. Neese, R. Izsák, *J. Chem. Phys.* **2018**, *148*.

Manuscript received: July 2, 2025
Version of record online: August 23, 2025

© 2025 The Author(s). European Journal of Organic Chemistry published by Wiley-VCH GmbH